PHYSICAL REVIEW B VOLUME 50, NUMBER 7 15 AUGUST 1994-I

Tunneling spectroscopy of the (110) surface of direct-gap III-V semiconductors

R. M. Feenstra
IBM Thomas J. Watson Research Center, P.O. Box 218, Yorktown Heights, New York 10598
(Received 18 April 1994)

Results of tunneling spectroscopy measurements of the (110) cleaved surface of GaAs, InP, GaSb, InAs, and InSb are presented. These materials form the family of direct-gap III-V binary semiconductors. Spectroscopic measurements are performed in ultrahigh vacuum, using a scanning tunneling microscope (STM). Techniques based on variable tip-sample separation are used to obtain high dynamic range (six orders of magnitude) in the measured current and conductance. Detailed spectra are obtained for all the materials, revealing the conduction- and valence-band edges, onset of the higher lying conduction band at the L point in the Brillouin zone, and various features associated with surface states. The precision and accuracy in determining energetic locations of spectral features are discussed. In particular, limitations in the accuracy due to tip-induced band bending is considered.

I. INTRODUCTION

Spectroscopic measurements with the scanning tunneling microscope (STM) were an important element in the development of the STM field.[1] These early spectra, acquired on surfaces such as Si(111)7×7 and Si(111)2×1,[2–4] were dominated by the presence of surface-state features, and indeed the goal of the measurement was to deduce the electronic state spectrum of the particular surface. Later measurements on GaAs(110) surfaces[5] revealed the signature of the *bulk* band gap in the spectrum, consistent with the knowledge that the dangling-bond states on that surface do not appear in the gap.[6] This lack of states within the band gap for GaAs(110) then opened the way to STM studies of the introduction of states in the gap due, e.g., to metal deposition.[7] Cross-sectional studies of GaAs-based structures soon followed,[8–10] and such studies of III-V epitaxial layers and superlattices are presently an active research area.

In this work, we present detailed STM spectroscopic measurements of the (110) cleaved surface of GaAs, InP, GaSb, InAs, and InSb. These materials form the family of direct gap III-V binary semiconductors. The motivation for this work is to obtain a detailed understanding of all the spectra, which is then useful for interpreting other spectra obtained, e.g., from alloys, thin quantum wells, or other structures. We find that a comprehensive study across this range of materials enables us to identify clearly the observed spectral features. Although considerable tunneling spectroscopy for GaAs has previously been presented,[5,9] only a few results (with relatively low spectral quality) are available for the other materials.[11,12]

For our measurements, we use a technique based on continuously variable tip-sample separation to achieve high dynamic range (six orders of magnitude) in the measurement of current and conductance. Subsequent analysis of the spectra by normalizing the differential conductance to the total conductance then permits clear identification of all the spectral features on a linear scale. These acquisition and analysis methods have been previously described,[13] and we summarize the relevant details here. With these techniques, we obtain detailed spectra for all the materials studied, with high spectral quality. The spectra reveal the conduction- and valence-band edges of the semiconductors, the onset of the higher-lying conduction band at the L point in the Brillouin zone, and various surface-state-derived features. In most cases the energetic locations of these features are already known from other methods, and good agreement is found with our STM results. We discuss the precision with which spectral positions can be determined (typically ± 0.03 eV), and the reproducibility of the measurement when different samples and probe tips are used (typically ± 0.05 eV). Thorough *in situ* cleaning of the probe tips is essential for obtaining reproducible spectra, and our tip preparation procedures are described. We consider systematic errors in spectral positions due to tip-induced band bending, which, for doping concentrations greater than 1×10^{18} cm^{-3}, are found to be generally less than 0.1 eV.

This paper is organized as follows. Section II summarizes experimental details, and spectroscopic techniques are described in Sec. III. Section IV presents the spectra of the various materials, and gives results about the variation of the spectra with different tips and samples. The effects of tip-induced band bending on the spectra are analyzed in Sec. V, and a discussion of the spectral features is given in Sec. VI. The paper is summarized in Sec. VII.

II. EXPERIMENT

The STM used for these experiments has been described previously.[14] It is contained in an ultrahigh-vacuum (UHV) system with pressure of $<4\times 10^{-11}$ Torr. Facilities for *in situ* sample and tip transfer, sample cleavage, and tip cleaning and inspection, are available. Samples measuring 0.1×0.7 in. are cut from the semiconductor wafers, and Au-Ge ohmic contacts are deposited on both sides. The samples are mounted in sample holders with half of the sample (0.35 in.) protruding from the holder. Cleavage is accomplished by *in situ* describing a notch, 0.02 in. long, on the face of the sample, and

0163-1829/94/50(7)/4561(10)/$06.00 ©1994 The American Physical Society

pressing on this face to initiate the cleave. Ideal cleaves of a (110) crystal face are obtained, which appear optically flat with almost no steps.

Semiconductor wafers used in these experiments were obtained from a wide variety of commercial sources, with the wafers generally being substrate material for epitaxial growth studies. In a few cases the results presented here were obtained from thin films grown by molecular-beam epitaxy, with the thickness of the films being much greater than a depletion width in the material. The semiconductor doping type and concentration were known from the manufacturer's specifications, and in all cases those values were checked using either secondary ion mass spectrometry (SIMS), four-point-probe resistivity, or the room-temperature Hall effect. Doping concentrations for the samples discussed here are as follows: GaAs, $n=1\times10^{19}$ cm^{-3} and $p=5\times10^{19}$ cm^{-3}; InP, $n=9\times10^{18}$ cm^{-3}; GaSb, $p=1\times10^{19}$ cm^{-3}, InAs, $n=9\times10^{17}$ cm^{-3}; and InSb, $n=2\times10^{17}$ cm^{-3}. In addition to the above samples, we also studied some lower doped material, with doping concentrations of GaAs, $n^{-}=2\times10^{16}$ cm^{-3} and GaSb, $p^{-}=2\times10^{17}$ cm^{-3}.

Single-crystal ⟨111⟩-oriented tungsten tips are electrochemically sharpened using microetching techniques.[15] Cleaning is performed *in situ* using electron bombardment, in which the tip is positioned inside a coiled, hot filament, and typically 2.5 mA of emission current is passed between tip and filament with +500-V bias on the tip. This procedure is repeated a few times. Subsequent inspection of the tips is performed by field-emission microscopy. We obtain an image of the tip on a microchannel plate using a bias voltage on the tip typically in the range −300 to −600 V. Comparing with field-emission formulas for a current of about 10 pA, this implies a radius of curvature of the tip in the range 300–600 Å.[16] However, the field-emission image itself usually reveals only a few atoms on the tip apex contributing to the emission current (more extensive heating produces blunter tips, which then reveal conventional field-emission patterns with hundreds of atoms arranged in crystalline planes). The occurrence of only a few atoms in a field-emission pattern, arising from a small protuberance on the surface, is known to decrease the field-emission voltage for given current by a factor 2–3.[17] Thus for the cleaning procedure given above, we find that the probes consist of ~1000-Å radius-of-curvature tips, on top of which there exist smaller "minitips" with ~10-Å radius of curvature.

III. SPECTROSCOPIC TECHNIQUE

Spectroscopic measurements are performed using variable tip-sample separation, as described previously.[13,18,19] These methods yield a dynamic range of about six orders-of-magnitude in the measurement of current and conductance, which is required for a clear definition of all the spectral features. An example of the raw data from such a measurement is shown in Fig. 1. We measure the tunnel current $I_m(V)$ [Fig. 1(a)], and conductance $(dI/dV)_m$ [Fig. 1(b)], where the subscript m refers to the *measured* quantity. The conductance is measured with a lock-in

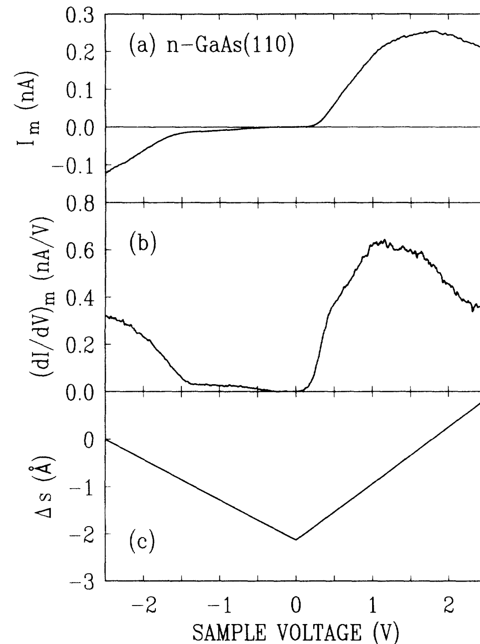

FIG. 1. Raw data from an *n*-type GaAs(110) surface, showing the (a) measured tunnel current and (b) measured conductance, as a function of sample voltage. The applied variation in tip-sample separation is shown in (c).

amplifier, using typically 50-mV modulation at 1 KHz on the bias voltage (at each voltage V, the conductance is thus the *partial* derivative of current with respect to voltage for fixed tip-sample separation).[13] Measurement of a spectrum requires several seconds. As the voltage between sample and tip is scanned, the tip-sample separation s is varied along some user-specified contour, as shown in Fig. 1(c). We use a contour of the form

$$s(V)=s_0+a|V| , \tag{1a}$$

where $s_0\equiv s(0)$. In practice, we specify tip displacements relative to that at the starting voltage V_1 of the spectrum, from which

$$\Delta s(V)\equiv s(V)-s_1=s_0-s_1+a|V| , \tag{1b}$$

where $s_1\equiv s(V_1)$. The constant a is chosen to amplify the current and conductance at low voltages up to some conveniently measurable level. A typical value for a is 1 Å/V, and slightly different values may be used for positive and negative voltages (i.e., an asymmetric V-shaped contour) to permit accurate measurement of both sides of the spectrum. The form of Eq. (1) is chosen for convenience in performing the measurement. Of course, data can also be acquired at constant tip-sample separation, and with suitably long integration times a high dynamic range in the conductance can be achieved. The advantage of our variable separation method is that the conductance at low voltage is amplified (with the noise level remaining the same), so that an extra 2–3 orders of magnitude in dynamic range is achieved with no additional acquisition time.

Analysis of the spectral data proceeds in two steps.

First, we transform the data to constant tip-sample separation using the well-known form for the dependence of current (and conductance) on separation,

$$I=I_0 \exp(-2\kappa s) , \tag{2}$$

where, to lowest order, κ is independent of s and V. For ideal vacuum tunneling κ has a value of $\sqrt{(2m\phi/\hbar^2)}=1.1$ Å^{-1} for an average work function of $\phi=4$ eV of tip and sample. In practice, observed values of κ may be less than this due to the nonideal behavior of the tunnel junction. We generally observe values of κ in the range 0.7–1.1 Å^{-1}, although in unusual cases the values may be lower than this due to an anomalous probe tip, and such a tip is then recleaned or discarded. Experimental values of κ are obtained by measuring current vs separation [Fig. 2(a)], and fitting those curves to an exponential form, yielding the κ values shown by the open circles in Fig. 2(b). There exists a more sophisticated method, based on partial derivatives, for determining κ directly from the observed spectrum.[20] Results from that method are shown by the solid line in Fig. 2(b), and they are in good agreement with those obtained from the $I_m(s)$ measurements. The observed values for κ are found to be relatively independent of voltage, and thus transformation of the observed spectra to constant s is accomplished by

$$I_S(V)=I_m(V)\exp(2\bar{\kappa}\Delta s) , \tag{3a}$$

$$\left[\frac{dI}{dV}\right]_S = \left[\frac{dI}{dV}\right]_m \exp(2\bar{\kappa}\Delta s) , \tag{3b}$$

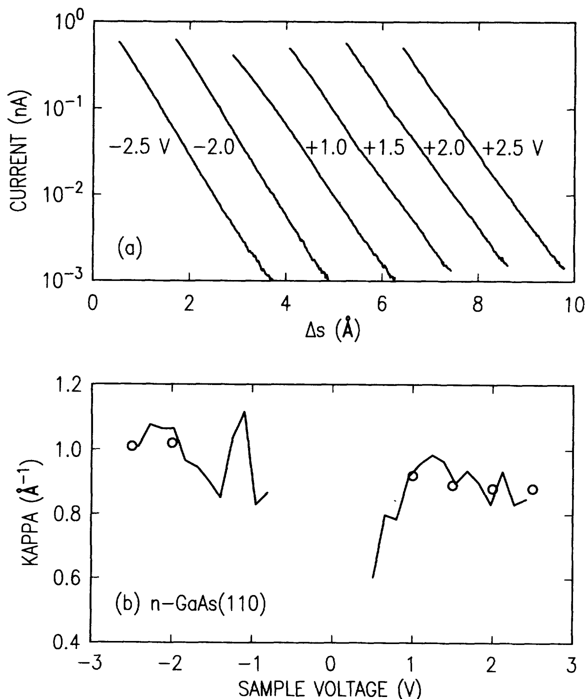

FIG. 2. (a) Measured current vs tip-sample separation, at various sample voltages indicated. (b) One-half of the exponential decay constant of the tunnel current, obtained from fitting the $I_m(s)$ curves of (a) (open circles), and from analysis of the spectral data of Fig. 1 (solid line).

where $\bar{\kappa}$ is the observed value of κ averaged over voltage. An example of this procedure, for the n-type GaAs raw data of Fig. 1, is shown by the solid line in Fig. 3(a), using a value of $\bar{\kappa}=0.93$ Å^{-1} obtained from the $I_m(s)$ measurements of Fig. 2. Similarly, constant-s conductance for p-type GaAs is shown in Fig. 4(a). In both cases, the dynamic range of the conductance extends over 5–6 orders of magnitude. This large range is required for application of the second step of the analysis, described below.

The second step in the analysis is to normalize the differential conductance (dI/dV) to the total conductance (I/V). The ratio of these quantities has been previously demonstrated to provide a very convenient measure of surface-state density for the case of metallic or small-band-gap surfaces.[13,21,22] However, for large-band-gap surfaces, the ratio $(dI/dV)/(I/V)$ diverges at the band edges, simply because the current approaches zero faster than the conductance.[18] This divergence is undesirable from the point of view of obtaining an experimental approximation of the surface-state density. Various authors have overcome the divergence problem simply by adding a small constant to I/V, or by applying some amount of broadening to the I/V values.[13] We employ the latter method here, forming $\overline{I/V}$, which is the total conductance broadened or smoothed over voltage.

Without broadening of I/V, the normalized conductance $(dI/dV)/(I/V)$ would have practically the same

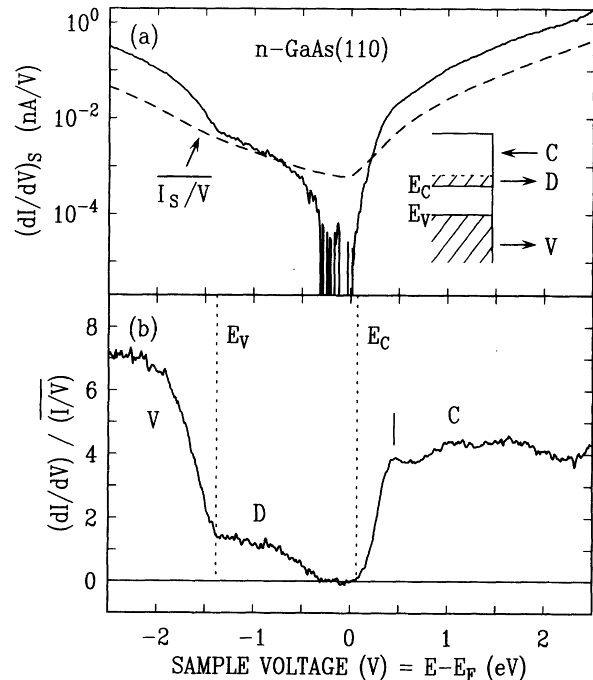

FIG. 3. Analyzed spectral data for n-type GaAs(110), showing (a) the differential conductance at constant tip-sample separation, and (b) the ratio of differential to total conductance. The dashed line in (a) shows the total conductance, broadened over a voltage width of 1.5 V. The components of the spectrum are indicated in the inset: C—conduction band, V—valence band, and D—dopant induced. Valence- and conduction-band edges are indicated by dotted lines, labeled E_V and E_C, respectively. The thin vertical line at 0.45 V marks a surface-state feature.

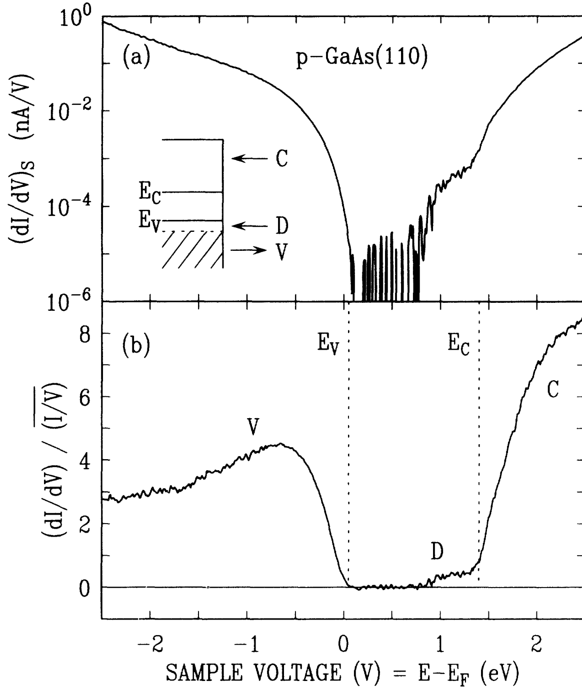

FIG. 4. Analyzed spectral data for p-type GaAs(110), showing (a) the differential conductance at constant tip-sample separation, and (b) the ratio of differential to total conductance. The components of the spectrum are indicated in the inset: C—conduction band, V—valence band, and D—dopant induced. Valence- and conduction-band edges are indicated by dotted lines, labeled E_V and E_C, respectively.

value when computed using either measured or constant-s quantities, since the ratio of conductance to current is nearly independent of tip-sample separation. With the broadening, however, care must be taken in which quantities are used. Let us first consider forming the normalized conductance $(dI/dV)_m/(\overline{I_m/V})$ using the *measured* current and conductance. A suitable method for broadening I_m/V would be to convolute it with, e.g., a Gaussian or exponential function. We choose the latter here, defining

$$\overline{I_m/V} \equiv \int_{-\infty}^{\infty} [I_m(V')/V'] \exp\left\{\frac{-|V'-V|}{\Delta V}\right\} dV' , \quad (4)$$

where ΔV is the broadening width. The value of ΔV should be on the order of the band gap of the material in order to suppress noise contributions in the middle of the gap due to the normalization procedure.[18] The overall shape of the spectra, and the position of spectral features, are insensitive to the value chosen for ΔV.[18] In previous studies of GaAs we used $\Delta V = 1.5$ V, and we take this same value here for normalization of all the spectra from various materials.

Two minor technical details arise in the computation of $\overline{I_m/V}$ in Eq. (4). First, for small voltages near 0 V, where the measured current and conductance are below the noise level, their ratio is extremely noisy and divergent. This situation is avoided by using in the integrand of Eq. (4) values for I_m which have been set identically equal to zero for the voltage range where the measured current is below its noise level. The subsequent broadening of I_m/V then produces a smoothly varying function with nonzero values throughout the band gap, which forms a suitable normalization quantity. Second, when applying the integral in Eq. (4) at high voltages outside the measured range, we must somehow extend the values of I_m to these voltages. This is done simply by extending the I_m values with a constant value equal to the value of I_m at the largest measured voltage (the extension is done separately for positive and negative voltages).

Examples of the normalized conductance, for n- and p-type GaAs, are shown in Figs. 3(b) and 4(b), respectively. A number of features are resolved in the spectra. Valence- and conduction-band onsets are clearly defined, denoted by E_V and E_C, respectively. The zero of voltage corresponds to the Fermi-level position in the semiconductor, seen to be located at the top (bottom) of the band gap for n-type (p-type) material. Nonzero current and conductance within the gap, the so-called "dopant-induced" component, arises from electrons tunneling out of filled conduction-band states for n-type material or into empty valence-band states for p-type material.[5] The relevant states contributing to this conductance are located very near the band edges, of course, but due to the voltage dependence of the tunneling transmission term, contributions to the conductance from these states are seen throughout the band gap. This D component in the conductance is a very sensitive measure of surface quality, since a small shift in surface Fermi-level position due to steps or residual contamination will cause this component to disappear from the spectrum, as described in detail elsewhere.[23] Other features which are visible in the spectra are small bumps seen on the empty-state (positive voltage) side of the spectrum, as marked by the vertical line in Fig. 3(b). We interpret these features as arising from cation-derived surface states, as discussed in Sec. IV.

In practice, our normalization of differential to total conductance is performed using measured, variable-s data, as in Eq. (4). However, since a number of workers acquire data with fixed tip-sample separation (due to constraints of their equipment), it is important to have a procedure which will produce similar results when applied to constant-s quantities. Let us consider broadening I_S/V in a manner similar to that described above. A problem arises in this procedure due to the fact that $I_S(V)$ for a large-gap semiconductor increases very rapidly (exponentially) with voltage, and thus broadening of the function will tend to heavily weight values of the current from higher voltages. This problem can be overcome by introducing a weighting factor in the broadening procedure itself, which suitably scales the values of I_S. The inverse weighting procedure is, of course, applied after the broadening. With these considerations, a suitable normalization quantity is defined to be

$$\overline{I_S/V} \equiv \exp(a'|V|) \int_{-\infty}^{\infty} [I_S(V')/V'] \exp\left\{\frac{-|V'-V|}{\Delta V}\right\} \times \exp(-a'|V'|) dV' . \quad (5)$$

The weighting function here is $\exp(-a'|V|)$ where a' is chosen to approximately equal the average exponential slope of $I_S(V)$, typically 2 V^{-1}. Because of this choice of exponential weighting, a simple relationship is obtained between normalization terms computed using either measured or constant-s quantities. To derive this relationship, we write $\overline{I_S/V}$ in terms of $\overline{I_m/V}$ by substituting Eqs. (1) and (3a) into Eq. (5), and comparing with Eq. (4). Without loss of generality we can take $a'=2\bar{\kappa}a$ (since a' is a free parameter), yielding

$$\overline{I_S/V}=\exp[2\bar{\kappa}(s_0-s_1+a|V|)]\overline{I_m/V} . \quad (6)$$

An example of this quantity, for the n-type GaAs data, is shown by the dashed line in Fig. 3(a). We see that the normalization term is a smoothly varying function of voltage, and it acts simply to rescale the magnitude of the differential conductance, so that their ratio can be viewed on a linear scale. To compare the results of normalization using either variable-s or constant-s quantities, we combine Eqs. (1), (3b), and (6), to yield

$$\frac{(dI/dV)_S}{(\overline{I_S/V})}=\frac{(dI/dV)_m}{(\overline{I_m/V})} . \quad (7)$$

Thus, in principle, identical results are obtained in the normalized conductance using either variable-s or constant-s quantities. In practice, the variable-s results will be of higher quality, since $(dI/dV)_S$ obtained from Eq. (3b) generally has a better signal-to-noise ratio than that measured directly using constant s. Because of the equality expressed by Eq. (7), we drop the subscripts m or S in the normalized conductance, denoting it simply as $(dI/dV)/(\overline{I/V})$.

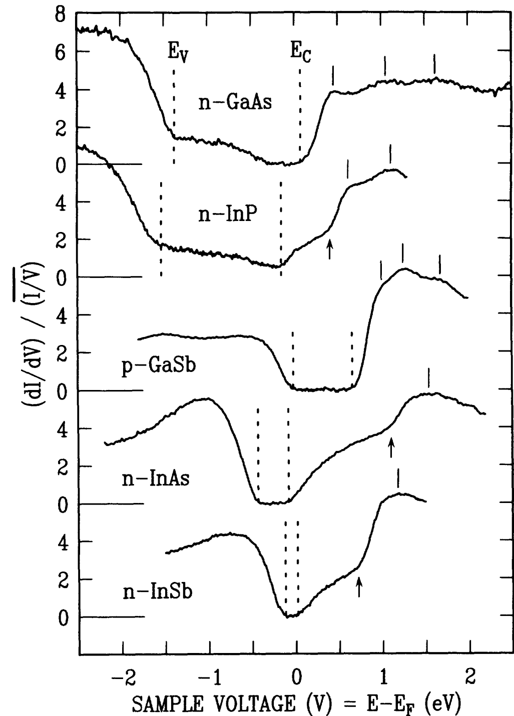

FIG. 5. Tunneling spectroscopy of the (110) surface of GaAs, InP, GaSb, InAs, and InSb. Valence and Γ-valley conduction-band edges are indicated by dotted lines, labeled E_V and E_C, respectively. Onset of the L-valley conduction band is indicated by an upward pointing arrow. Surface-state peaks are marked by thin vertical lines. The sample voltage corresponds to the energy of a state relative to the Fermi level.

IV. RESULTS

In Fig. 5 we show the major result of this paper—high quality spectroscopic data obtained from the (110) surface of GaAs, InP, GaSb, InAs, and InSb. Each of the curves consists of an average of 2–10 spectra, acquired individually and averaged together to improve the signal-to-noise ratio. As described in Sec. III, all spectra are acquired with $s(V)$ ramp slope of $a \simeq 1$ Å/V [Eq. (1)], and normalization of differential to total conductance is performed using $\Delta V = 1.5$ V broadening of the total conductance [Eq. (4)]. Detailed spectra from each material in Fig. 5 are obtained. Band gaps are clearly resolved in the spectra, marked by dotted lines, with known values of 1.42, 1.34, 0.72, 0.36, and 0.17 eV at room temperature for GaAs, InP, GaSb, InAs, and InSb, respectively.[24–29] For the cases of InP, InAs, and InSb, we observe an additional onset above the lowest conduction band, as marked by the upward pointing arrows in Fig. 5. Based on the position of these onsets, we identify them as arising from the indirect conduction-band minimum centered at the L point in the Brillouin zone. This L-point onset is not seen for GaSb, since its conduction-band minima at the Γ and L points are separated by only 85 meV,[28] and it is not seen for GaAs due to overlapping contributions from surface states, as discussed below.

Onset energies for band extrema are determined by assuming linear onsets in the normalized conductance. Examples of applying this procedure are shown in Fig. 6. Straight lines are drawn through the data on either side of the onset, and the onset energy is given by the intersection of the lines. In most cases, a linear region in normalized conductance is observed for at least several tenths of an eV on either side of the onset, as in Figs. 6(a), 6(c), and 6(d), so that the onset energy is easily determined. In a few cases, the normalized conductance is more curved near the onset, as in the high-energy side of Fig. 6(b). In those cases, a linear portion of the conductance is assumed to exist over a width of about 0.1 eV, and a straight line is drawn through that portion of the spectrum. The precision of onset energies determined by this method is estimated to be ±0.03 eV. A summary of the observed valence- and conduction-band onsets is given in Table I.

In addition to the band onsets, small peaks are observed in the spectra. These peaks are seen on the empty state side, and we associate them with cation-derived density-of-state (DOS) features. These features may be bulk or surface related, although we generally expect sharp features to arise from states (resonances) with some significant surface character. These peaks are marked by vertical lines in Fig. 5, located with a precision of ±0.03 eV. The surface states form distinctive series for GaAs, InP, and GaSb, with a sharp feature seen at 0.45 V for GaAs, two sharp features seen at 0.62 and 1.11 V for InP,

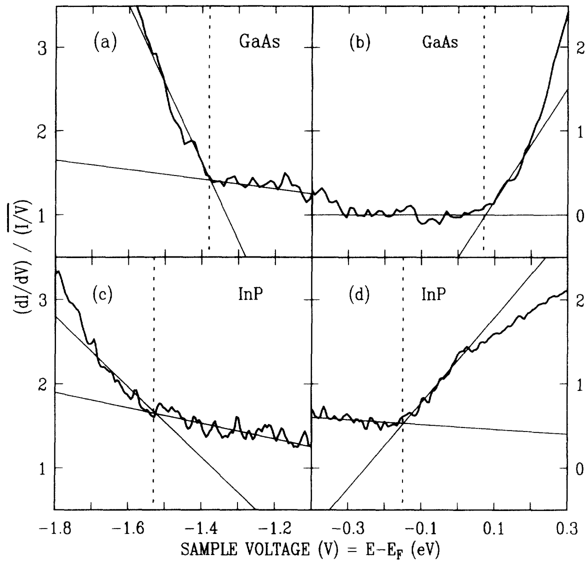

FIG. 6. Examples of determination of band onset positions, for the various materials indicated. Straight lines are drawn through the spectra on either side of an onset, and the onset position is given by the intersection of the lines.

and a triplet of surface states seen at 1.00, 1.25, and 1.68 eV for GaSb. The intensity of these features varies from spectrum to spectrum, but their energetic location is relatively constant, as discussed in more detail below. For the cases of InAs and InSb, only a single broad maximum is observed above the L-valley onset. This maximum in each spectrum persists even if the data are analyzed with $\Delta V=0$, indicating that it is a *bona fide* DOS feature. The energetic locations of observed surface state features are summarized in Table I. In some cases, surface-state features can obscure the observation of bulk band onsets. This is believed to occur for the GaAs spectrum of Fig. 5, where we do not see the onset of the L valley [expected to occur 0.29 V above E_C (Ref. 24)] due to the presence of the surface states at 0.45 V. For the case of InP, a distinct surface state occurs at 0.62 V, just above the L-valley onset. This peak could in principle distort the L-valley onset position. However, in examining many spectra where the intensity of the 0.62-V surface state varies, we find that the onset position remains relatively constant, so we confidently assign it to the L-valley conduction-band minimum.

The position and identification of our observed spectral features are summarized in Table I. The results are displayed graphically in Fig. 7, where we consider the energetic locations relative to the observed valence-band maximum (assuming a normal distribution of errors, these energy differences have uncertainties of $\pm\sqrt{2}\,0.03\simeq\pm0.04$ eV). We compare our observations with the positions of bulk- and surface-derived electronic states known from other measurements.[24–34] Good agreement is found for the positions of the Γ- and L-valley conduction bands, thus confirming their identification. As noted by Fischetti, significant uncertainty exists in some of the previously known L-valley positions,[25] with the uncertainty generally increasing as we move from GaAs to InSb in Fig. 7. We find that the STM results provide a measurement accuracy comparable to previous results for most of the materials. For InSb in particular, our STM L-valley minimum location of 0.84 ± 0.04 eV relative to E_V (or 0.70 ± 0.04 eV relative to E_C) is, to our knowledge, the first experimental determination of this energy (the "known" value plotted in Fig. 7 is based on a theoretical estimate.[30])

For surface states, we find generally good agreement between our STM peak locations and previous inverse photoemission results. The inverse photoemission results plotted in Fig. 7 are the energies at various critical points in the Brillouin zone, and thus they need not agree precisely with the DOS maxima locations seen by STM, which may form at interior points in the zone. For GaAs, the two surface states at $E=E_V+1.83$ and 2.43 eV agree with the location of the lowest surface band seen in inverse photoemission, and the state observed at $E=E_V+3.00$ eV is consistent with an upper surface band.[31] Similarly, good agreement is seen in Fig. 7 between the STM and inverse photoemission results for the sharp features seen for InP and GaSb,[32,33] and for the broad feature observed for InAs.[34] The STM and inverse photoemission results do not agree for the surface-state position in InSb,[34] and more experimental work is required to resolve this difference.

Reproducibility of the STM results is illustrated in Figs. 8 and 9. For GaSb and GaAs, we show four spectra each, with all spectra acquired from different samples using different probe tips. The spectra from a given material all show generally the same band-gap and surface-state features, marked by dotted and vertical lines, respectively. The location of the surface Fermi level (0 V) within the gap varies, as does the intensity of the midgap D component seen for GaAs. Both of these quantities are very

TABLE I. Peak positions (eV) relative to E_F of STM spectral features for GaAs, InP, GaSb, InAs, and InSb(110) surfaces. Random errors are ±0.03 eV, and systematic errors due to tip-induced band bending are less than 0.1 eV.

GaAs	InP	GaSb	InAs	InSb	Identification
−1.38	−1.53	−0.02	−0.43	−0.12	E_V, valence-band maximum
0.07	−0.15	0.66	−0.08	0.02	E_C, Γ-valley minimum
	0.41		1.10	0.72	L-valley minimum
0.45	0.62	1.00	1.54	1.18	surface DOS features
1.05	1.11	1.25			surface DOS features
1.62		1.68			surface DOS features

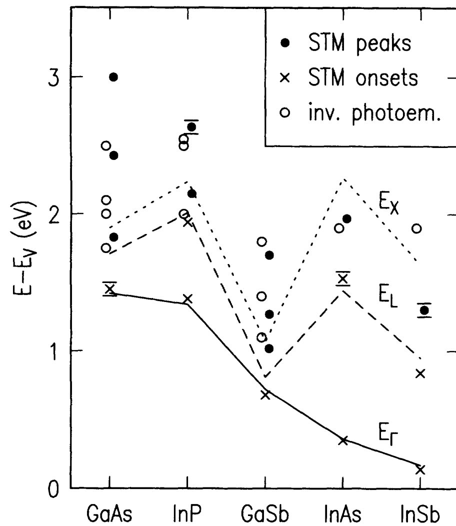

FIG. 7. Summary of observed energies, relative to the valence-band maximum (E_V). Tunneling spectroscopy results for onsets are shown by x marks, and for peak positions by solid dots. Error bars for random uncertainties (± 0.04 eV) are shown on a few points; systematic uncertainties are less than 0.1 eV. Inverse photoemission results for surface states are shown by open circles (from Refs. 31–34). Bulk conduction-band edges, known from other methods (Refs. 24–30), are shown by solid, dashed, and dotted lines for Γ, L, and X valleys, respectively.

sensitive to the presence of residual defects on the surface (as discussed in Sec. III) and also depend on the relative work functions between tip and sample. For a fixed doping concentration, the energetic position of surface states varies by typically ± 0.05 eV for different tips and samples. The peak heights depend slightly on spatial position

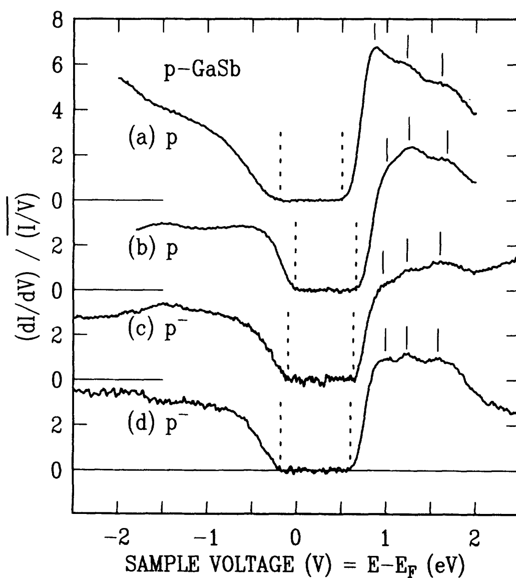

FIG. 8. Variation in spectroscopic results, for p-type GaSb. Each spectrum was acquired from a different sample, using a different probe tip. Doping concentrations are $p = 1\times 10^{19}$ cm^{-3} and $p^- = 2\times 10^{17}$ cm^{-3}.

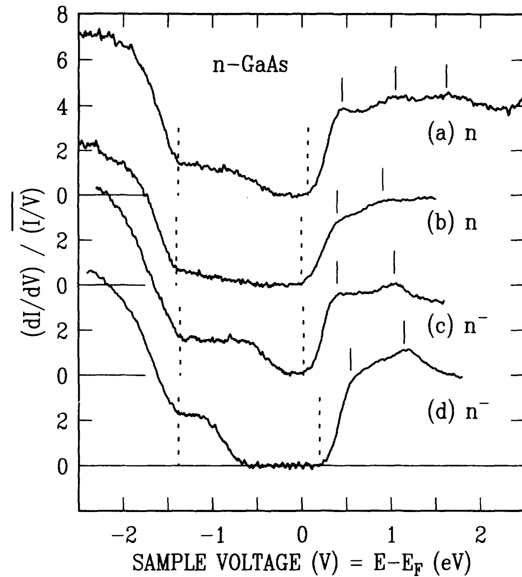

FIG. 9. Variation in spectroscopic results, for n-type GaAs. Each spectrum was acquired from a different sample, using a different probe tip. Doping concentrations are $n = 1\times 10^{19}$ cm^{-3} and $n^- = 2\times 10^{16}$ cm^{-3}.

on the surface (i.e., over a cation or anion), and vary significantly with different probe tips. An example of the latter is seen in GaSb spectrum of Fig. 8(a), which appears quite different than the others, with the lowest surface state being relatively intense. We attribute this difference to a distortion arising from the electronic properties of the probe tip itself. Even with these tip-to-tip variations, it is still relatively easy to measure spectra from identical samples using several different tips, and thereby determine spectral positions to an accuracy which falls within the ± 0.03-eV precision range mentioned above.

In addition to the uncertainty arising in spectral determination due to different tips and samples, it is also possible that the spectra may be distorted due to tip-induced band bending in the semiconductor.[5] This effect will, of course, depend on the doping concentration in the semiconductor. Theoretical estimates of this effect are given in Sec. V, and here we examine experimental data for various doping concentration, as shown in Figs. 8 and 9. In Fig. 8, the p-type GaSb doping concentration was 1×10^{19} cm^{-3} for Figs. 8(a) and 8(b), and 2×10^{17} cm^{-3} for Figs. 8(c) and 8(d). Comparing the lower-doped to the higher-doped material, we find that, on average, the band gap is 0.07 eV larger and the surface states are shifted up in energy by 0.04 eV. These values are relatively small, being in the range of random sample-to-sample and tip-to-tip errors. But the values are consistently observed in the spectra from differently doped materials, and thus we attribute them to tip-induced band-bending effects. In Fig. 9, the n-type GaAs doping concentration was 1×10^{19} cm^{-3} for Figs. 9(a) and 9(b), and 2×10^{16} cm^{-3} for Figs. 9(c) and 9(d). In this case, spectrum (c) from the lower-doped material is almost identical to the spectra of the higher-doped material, but spectrum (d) has band-gap and surface-state energies which are about 0.15 eV larger

than the others. We attribute this shift to tip-induced band bending. For low doping concentrations $\lesssim 1\times 10^{17}$ cm^{-3}, the magnitude of these effects is found to vary significantly from tip to tip. This observation is consistent with that reported by Maboudian *et al.*,[35] and is presumably due to varying radius of curvature and work function of the tips. Such large variation ($\gtrsim 0.2$ eV) in spectroscopic results is *not* observed for higher doping concentrations $\gtrsim 1\times 10^{18}$ cm^{-3}.

V. TIP-INDUCED BAND BENDING

In the STM, the proximity of a metal probe tip to a semiconducting sample can lead to large amounts of tip-induced band bending in the semiconductor.[5] The voltage drop between the tip and sample surface is thus less than the applied sample-tip voltage V, thereby affecting the accuracy of the spectroscopic energy scale $E-E_F(\text{eV})=V(\text{V})$. An important effect which must be considered here is the occurrence of electron tunneling through the depletion region of the semiconductor. Because of this effect the potential barrier produced by the band bending is partially transparent to the electrons, and thus the influence of tip-induced band bending on the tunnel current is significantly reduced. This point was considered by Feenstra and Stroscio using a one-dimensional model (1D),[5] which provided an upper limit on the tip-induced band-bending effects. More recently, several authors have suggested the importance of using a 3D model to understand tip-induced band bending.[35–37] Below we describe some computations for electron depletion layer tunneling, in a 3D geometry, which establish limits on the effect of tip-induced band bending on tunneling spectra.

We consider a sharp probe tip, consisting of a 10-Å radius hemisphere on a 500-Å radius-of-curvature paraboloid, located 10 Å from a semiconductor. This model of a tip was suggested by McEllistrem *et al.*,[37] and is consistent with our tip geometry determined from field emission, as discussed in Sec. II. We solve for the electrostatic potential distribution numerically, for the semiconductor in depletion with an applied sample-tip bias voltage of 1 V relative to flat-band conditions. Results for the potential along the axis of cylindrical symmetry in the semiconductor are shown in Fig. 10(a). The tip-induced band bending on the semiconductor surface is denoted $e\Delta V$, and results for this quantity as a function of doping concentration are shown in Fig. 10(c). We see that the tip-induced band-bending effects are relatively large, especially at low doping, consistent with previous 1D results[5] (3D surface band bending is about 40% smaller than in 1D, because of the larger divergence of the potential in 3D).

To fully evaluate the effects of tip-induced band bending on the tunneling spectrum, one should perform a computation of tunnel current vs voltage, as done in Ref. 5 for 1D. However, such a computation in 3D is difficult, and not really required for the present purpose. Rather, we simply examine the transmission through the potential in the semiconductor. We consider the potential barrier as shown in Fig. 10(a), and compute the transmission

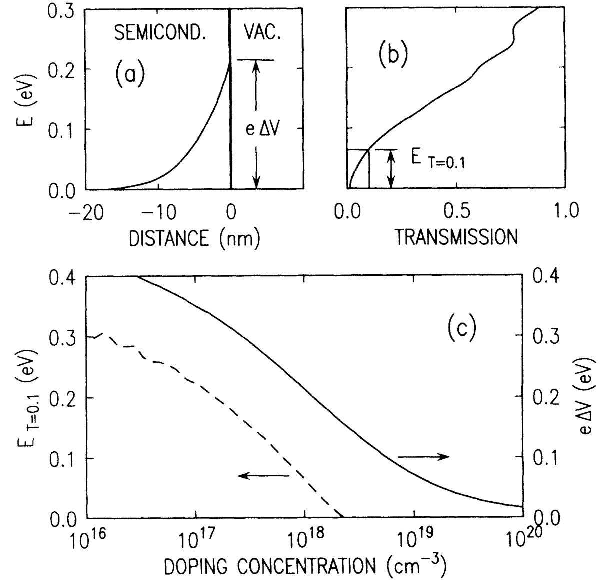

FIG. 10. (a) Tip-induced band bending in a semiconductor, for a fixed doping concentration of 1×10^{18} cm^{-3} and applied sample-tip bias of 1 V. The surface band bending $e\Delta V$ is shown. (b) Transmission probability as a function of energy, for the potential barrier shown in (a). The energy at which the transmission equals 0.1, $E_{T=0.1}$, is indicated. (c) The quantities $e\Delta V$ (solid line) and $E_{T=0.1}$ (dashed line) as a function of doping concentration.

probability of the barrier as a function of incident energy of a state relative to the conduction-band edge.[38] The results are shown in Fig. 10(b). Nonzero values of the transmission occur for states with energies less than $e\Delta V$ due to tunneling through the barrier. In terms of the onset of tunnel current at a band edge, a small value of transmission like 0.1 is sufficient to produce a clearly defined onset, because the current increases very rapidly with applied bias.[5] Thus we consider the energy at which the transmission equals 0.1, as shown by the dashed line in Fig. 10(c). We find that the effect of tip-induced band bending on the position of spectral onsets is $\lesssim 0.1$ eV for doping concentrations $>1\times 10^{18}$ cm^{-3}.

The above results provide an upper limit on the effects of tip-induced band bending on energetic positions observed in the tunneling spectra. In fact, the transmission value of 0.1 used above is conservative, since, with a large enough dynamic range in the current measurement, band onsets can be defined for much smaller values of the transmission. In addition, some adsorbates and/or defects are always present on the surface, and charging of such defects will act to pin the Fermi level and reduce the tip-induced band bending.[23] Also, the results of Fig. 10 apply to a semiconductor in depletion; band bending for accumulation (opposite bias) is, of course, much less.[5] Comparing the above theoretical estimates with the experimental results of Sec. IV, we conclude that, in practice, tip-induced band-bending effects for doping concentrations greater than 1×10^{18} cm^{-3} will generally be less than 0.1 eV. For doping concentrations in the range

1×10^{17} to 1×10^{18} cm^{-3}, tip-induced band bending can be as large as 0.1–0.2 eV, but it may also be smaller than this. For doping concentrations less than 1×10^{17} cm^{-3}, tip-induced band bending is expected to be generally several tenths of an eV or larger.

VI. DISCUSSION

In previous sections, we presented detailed tunneling spectra obtained from the family of III-V binary direct-gap semiconductors. Observed spectral features are identical as Γ-point valence- and conduction-band edges, the *L*-point conduction-band edge, and various surface states. The band edges are properties of the bulk material, and their observation provides a unique means of chemical identification of the particular material. Thus it is desirable to apply these types of measurements to a wider range of materials, and here we briefly consider the requirements for achieving this goal. By far the most important characteristic required for reproducible tunneling spectroscopy is a clean, ideal tunnel junction. Both the sample and probe tip must be prepared with clean surfaces, and this condition must be maintained during the measurement. The requirement of clean sample surfaces is no different than that encountered in other surface science measurements, and can generally be obtained using modern UHV techniques. Cleanliness of the probe tip can be accomplished using, e.g., the techniques described in Sec. II (most commercial STM manufacturers do not offer effective tip cleaning capabilities, and thus spectroscopic measurement is difficult with those instruments). A secondary requirement for obtaining high quality spectroscopic data is a high dynamic range (six orders of magnitude) in the measurement of tunnel current and conductance. Because of limitations in the magnitude of the tunnel current which can be measured without causing surface damage (0.1–1 nA, depending on material), this range is difficult to obtain in a single current vs voltage measurement at fixed tip-sample separation. The variable-separation method described in Sec. III provides a convenient means of overcoming this problem, and obtaining the required dynamic range (again, such methods are generally not available on commercial STM's). We note that the variable-separation methods are mainly applicable to ideal tunneling situations, i.e., when the voltage dependence of κ is not too large.

As noted in Sec. I, recent cross-sectional studies of epitaxially grown thin films and superlattices have demonstrated the significance of tunneling microscopy and spectroscopy in III-V semiconductor systems. Similar measurements should be possible on II-VI semiconductors, which, like the III-V's, are easily prepared by cleavage. Unfortunately, such detailed studies have not yet been possible on group-IV materials (Si, SiGe, etc.) due to difficulties in cleavage and passivation of the surface. For the case of the III-V's discussed in this work, we find that one limitation in the measurement arises from a type of glitchy noise which occurs in the tunnel current. For a given material and doping type, this noise will often arise when a particular sign and magnitude of bias is applied between the sample and tip. Once the noise starts, it is difficult to eliminate it without using another probe tip. This noise undoubtedly arises from the motion of electrons (through localized states) or atoms on the sample or the tip, but the precise mechanism is not known.

The *L*-point conduction-band minimum seen in our spectra is a relatively new feature in tunneling spectroscopy. In only one previous case, the measurements by Gwo *et al.* on sulfur-passivated GaAs(110) surfaces, were conduction-band minima above the lowest band observed.[10] The observation of multiple bands in tunneling might seem, at first glance, to be inconsistent with the old adage that "tunneling is not sensitive to (bulk) band structure".[39] In the context of the present measurements, however, this saying is better expressed as "each band contributes an equal amount to the tunnel current," with this equality arising from the well-known cancellation between density of states and velocity in the phenomenological theory.[39] Thus, neglecting details of wave-function matching at the semiconductor-vacuum interface, we expect the tunnel current from the *L* valley (or *X* valley) to be about the same magnitude as that from the direct Γ valley. This expectation is in contrast to the vastly different DOS for these bands, with the Γ valley having a much smaller DOS as characterized by its smaller effective mass.[25] This conclusion is consistent with our experimental results and those of Ref. 10, where similar size spectral features are seen for each of the bands. A remaining question concerns the *X*-valley conduction band, which is not seen in our spectra but does appear in Ref. 10. We attribute this difference to the overlapping effects of surface states in our case. As seen in Fig. 7, for GaAs, InP, and GaSb, the *X* valley lies just above the *L* valley, and its onset occurs at a position where we find a high density of surface-state features. For InAs and InSb the separation between *X* and *L* valleys is larger, and the effects of surface states appear to be smaller in the spectra. Additional studies of those materials may reveal spectral features from the *X* valley.

All the surface- and bulk-derived spectral features observed in this work occur in the conduction band, with no significant features seen in the valence band. One reason for this lack of valence-band structure may be the well-known energy dependence of the tunneling transmission term,[21] which preferentially weights empty-state features. In III-V semiconductors, the split-off valence band is located ~0.5 eV below the valence-band maximum E_V.[30] For GaSb, we observe a weak minimum in the spectra located ~1 eV below E_V, as seen in Figs. 5 and 8. Additional study is needed to determine whether this feature is associated with the split-off band or with some surface-derived states.

VII. SUMMARY

In this work, we have considered tunneling spectroscopy of the (110)-cleaved surface of GaAs, InP, GaSb, InAs, and InSb. High quality spectra are obtained in each case, using acquisition and analysis methods which rely on variable tip-sample separation. Bulk band gaps of

the materials, as well as the L-valley conduction-band edge and various DOS features attributed to surface states, are seen in the spectra. Precision in measuring spectral position, and reproducibility of the results from sample to sample and tip to tip are discussed. We conclude that, for a given sample type, spectral positions can be determined to ± 0.03 eV. Systematic errors in the measurement due to tip-induced band bending are considered in detail. We find that, for semiconductor doping concentrations of $\gtrsim 1 \times 10^{18}$ cm^{-3}, this effect produces spectral shifts which are generally less than 0.1 eV.

ACKNOWLEDGMENTS

Semiconductor materials used in this study were obtained from a variety of commercial sources, and from a number of research collaborators. We gratefully acknowledge J. M. Woodall, G. D. Pettit, D. A. Collins, T. C. McGill, and H. Munekata for providing these materials. We thank D. W. Kisker for assistance with Hall-effect measurements, and F. Cardone for SIMS measurements. We also thank F. Stern and M. V. Fischetti for useful discussions.

---

[1]For a review, see R. M. Feenstra, Surf. Sci. **299/300**, 965 (1994).

[2]R. S. Becker, J. A. Golovchenko, D. R. Hamann, and B. S. Swartzentruber, Phys. Rev. Lett. **55**, 2032 (1985).

[3]R. J. Hamers, R. M. Tromp, and J. E. Demuth, Phys. Rev. Lett. **56**, 1972 (1986).

[4]J. A. Stroscio, R. M. Feenstra, and A. P. Fein, Phys. Rev. Lett. **57**, 2579 (1986).

[5]R. M. Feenstra and J. A. Stroscio, J. Vac. Sci. Technol. B **5**, 923 (1987).

[6]S. Y. Tong, A. R. Lubinsky, B. J. Mrstik, and M. A. Van Hove, Phys. Rev. B **17**, 3303 (1978).

[7]R. M. Feenstra, Phys. Rev. Lett. **63**, 1412 (1989).

[8]H. W. M. Salemink, O. Albrektsen, and P. Koenraad, Phys. Rev. B **45**, 6946 (1992).

[9]A. Vaterlaus, R. M. Feenstra, P. D. Kirchner, J. M. Woodall, and G. D. Pettit, J. Vac. Sci. Technol. B **11**, 1502 (1993).

[10]S. Gwo, K.-J. Chao, C. K. Shih, K. Sadra, and B. G. Streetman, Phys. Rev. Lett. **71**, 1883 (1993).

[11]Ph. Ebert, G. Cox, U. Poppe, and K. Urban, Ultramicroscopy **42-44**, 871 (1992).

[12]L. J. Whitman, J. A. Stroscio, R. A. Dragoset, and R. J. Cellota, Phys. Rev. B **42**, 7288 (1990).

[13]*Scanning Tunneling Microscopy,* edited by J. A. Stroscio and W. J. Kaiser, Methods of Experimental Physics Vol. 27 (Academic, Boston, 1993), Chap. 4. There is a sign error in Eq. (17) of this work; the right-hand side should read $+a|V|$.

[14]R. M. Feenstra, in *Proceedings of the 21st International Conference on the Physics of Semiconductors,* edited by P. Jiang and H.-Z. Zheng (World Scientific, Singapore, 1992), Vol. 1, p. 357.

[15]A. J. Melmed, J. Vac. Sci. Technol. B **9**, 601 (1991).

[16]R. Gomer, *Field Emission and Field Ionization* (Harvard University Press, Cambridge, 1961), Eq. (51). There is a sign error in the exponent of the prefactor of this equation; it should read 6.2×10^{-6}.

[17]R. Gomer, *Field Emission and Field Ionization* (Ref. 16).

[18]P. Mårtensson and R. M. Feenstra, Phys. Rev. B **39**, 7744 (1988).

[19]C. K. Shih, R. M. Feenstra, and P. Mårtensson, J. Vac. Sci. Technol. A **8**, 3379 (1990).

[20]We apply Eq. (19) of Ref. 13, and compute $\kappa = -(\partial I / \partial s|_V)/(2I)$.

[21]R. M. Feenstra, J. A. Stroscio, and A. P. Fein, Surf. Sci. **181**, 295 (1987).

[22]N. D. Lang, Phys. Rev. B **34**, 5947 (1986).

[23]J. A. Stroscio and R. M. Feenstra, J. Vac. Sci. Technol. B **6**, 1472 (1988).

[24]J. S. Blakemore, J. Appl. Phys. **53**, R123 (1982).

[25]M. V. Fischetti, IEEE Trans. Electron Devices **38**, 634 (1991).

[26]J. Peretti, H.-J. Drouhin, D. Paget, and A. Mircéa, Phys. Rev. B **44**, 7999 (1991).

[27]A. G. Milnes and A. Y. Polyakov, Solid-State Electron. **36**, 803 (1993).

[28]H. J. Lee and J. C. Woolley, Can. J. Phys. **59**, 1844 (1981).

[29]Z. M. Fang, K. Y. Ma, D. H. Jaw, R. M. Cohen, and G. B. Stringfellow, J. Appl. Phys. **67**, 7034 (1990).

[30]J. R. Chelikowsky and M. L. Cohen, Phys. Rev. B **14**, 556 (1976).

[31]D. Straub, M. Skibowski, and F. J. Himpsel, Phys. Rev. B **32**, 5237 (1985).

[32]J. M. Nicholls, K. O. Magnusson, and B. Reihl, Surf. Sci. Lett. **243**, L31 (1991).

[33]H. Cartensen, R. Manzke, I. Schäfer, and M. Skibowski, in *Proceedings of the 18th International Conference on the Physics of Semiconductors,* edited by O. Engström (World Scientific, Singapore, 1987), p. 125.

[34]W. Drube, D. Straub, and F. J. Himpsel, Phys. Rev. B **35**, 5563 (1987).

[35]R. Maboudian, K. Pond, V. Bressler-Hill, M. Wassermeier, P. M. Petroff, G. A. D. Briggs, and W. H. Weinberg, Surf. Sci. Lett. **275**, L662 (1992).

[36]M. B. Johnson and J.-M. Halbout, J. Vac. Sci. Technol. B **10**, 508 (1992).

[37]M. McEllistrem, G. Haase, D. Chen, and R. J. Hamers, Phys. Rev. Lett. **70**, 2471 (1993).

[38]The transmission probability is defined as the ratio of surface wave functions with and without band bending, computed in a 1D approximation using those values of the 3D potential lying along the cylindrical symmetry axis of tip and sample, and assuming an effective mass of 0.1.

[39]C. B. Duke, *Tunneling in Solids* (Academic, New York, 1969).